COMMUNICATION

Ultrastable $Co_xSi_yO_z$ Nanowires by Glancing Angle Deposition with Magnetron Sputtering as Novel Electrocatalyst for Water Oxidation

Manuel Cano,*[a] Francisco J. Garcia-Garcia,[b,c] Daily Rodríguez-Padrón,[d] Agustín R. González-Elipe,[e] Juan J. Giner-Casares[a] and Rafael Luque*[d,f]

Dedication ((optional))

Abstract: Cobalt is one of the most promising non-noble metal as electrocatalyst for water oxidation. Herein, a highly stable silicon-cobalt mixed oxide thin film with a porous columnar nanostructure is proposed as electrocatalyst for oxygen evolution reaction (OER). CoO_x and $Co_xSi_yO_z$ layers with similar thickness were fabricated at room temperature by magnetron sputtering in a glancing angle configuration (MS-GLAD) on tin-doped indium oxide (ITO) substrates. After characterization, a comparative study of the electrocatalytic performance for OER of both layers was carried out. The excellent long-term stability as electrocatalyst for OER of the porous $Co_xSi_yO_z$ thin film demonstrates that the presence of silicon on the mixed oxide network increases the mechanical stability of the Si/Co layer, whilst maintaining a considerable electrocatalytic response.

Water oxidation or oxygen evolution reaction (OER) electrocatalysis has gained growing attention in recent years due to its key role in water splitting.[1–3] In general, this electrochemical reaction occurs at the anode both in acid (i.e. $2H_2O \rightarrow 4H^+ + 4e^- + O_2$) and in alkaline (i.e. $4OH^- \rightarrow 2H_2O + 4e^- + O_2$) electrolytes. The development of efficient, low-cost and durable electrocatalysts for OER is a current challenge for the definitive advance of this hydrogen energy storage technology. Different approaches containing Cobalt as electrocatalytic center material, such as chalcogenides[4–6], oxides[7–9], metal-organic frameworks (MOFs)[10–12] and layered double hydroxides (LDHs).[13–15] In addition, Cobalt can be supported onto conducting carbonaceous materials, e. g., graphene[16,17], reduced graphene oxide – RGO-,[18] nitrogen-doped RGO,[19] carbon nanotubes -CNTs-,[20] N-doped CNTs,[21] and electroconductive carbon black,[22] which is an interesting strategy to enhance the OER electrocatalytic performance by increasing the surface area, electrical conductivity and mass transfer rate.

Electrochromic materials and electrochromic energy storage devices are relevant Cobalt-based research fields, where color transformation implies the oxidation of cobalt cations and the incorporation of OH^- groups within the structure of the oxide (i.e. $CoO_x + OH^- \rightarrow CoO_xOH + e^-$).[23–26] This process corresponds to the step 1 of the proposed OER mechanism in alkaline medium, which is named formation of MOH intermediate.[2] The optimal performance of these type of thin film-based solid devices required a high porosity to allow a fast incorporation of OH^- groups within the layer and their reversible release to the electrolyte during the oxidation and reduction cycles. Recently, Garcia-Garcia et al. optimized the fabrication of $Co_xSi_yO_z$ electrochromic thin films by MS-GLAD,[27] previously used to fabricate $W_xSi_yO_z$,[28–30] demonstrating that this configuration provides excellent OH^- incorporation capacity and diffusion rate from the electrolyte medium. In addition, introducing Silicon into the mixed oxide network provides excellent mechanical and conductive features to the whole, even at high temperatures.[31] However, this technological approach has not yet been applied for water oxidation to the best of our knowledge.

In this prelaminar study, the potential use as OER electrocatalyst of CoO_x and $Co_xSi_yO_z$ thin films prepared by MS-GLAD method is evaluated (Scheme 1). Firstly, both layers were fabricated on ITO substrates according to the previously reported MS-GLAD procedure.[27] The porous $Co_xSi_yO_z$ and CoO_x layers were deposited using a 50 mm diameter Co/Si (75/25 wt%) and Co targets, respectively. In all cases, depositions were carried out using a $\phi_{O_2}/\phi_{Ar} = 0.1$ and target-substrate distance of 5 cm with an angle of 80 ºC between target and substrate normal.

Figure 1 shows the scanning electron microscope (SEM) images of CoO_x and $Co_xSi_yO_z$ samples, respectively. In both cases, the cross-section images confirm the expected nanocolumnar structure and the thickness of the resulting porous layers formed by MS-GLAD method. The top-view images evidence the porosity and the highly regular morphology obtained for both samples.

Energy-dispersive X-ray (EDX) measurement on SEM images was also performed for qualitative and semiquantitative analysis of chemical elements on the surface of both films (Figure 1E-J). The resulting SEM-EDX mapping confirmed the presence of Co and O in the CoO_x layer (see Table S1). Moreover, this analysis also showed the presence of silicon, cobalt and oxygen in the $Co_xSi_yO_z$ layer. As it was expected, the surface of the latter thin

[a] M. Cano, J.J. Giner-Casares
Department of Physical Chemistry & Applied Thermodynamics
Institute of Nanochemistry (IUNAN), University of Córdoba (UCO)
Campus Universitario de Rabanales, Córdoba 14014 (Spain)
E-mail: q82calum@uco.es
[b] F.J. García-García
Department of Inorganic Chemistry & Chemical Engineering
IUNAN, UCO
Campus Universitario de Rabanales, Córdoba 14014 (Spain)
[c] F.J. García-García
Department of Engineering & Materials Science & Transportation
University of Seville
Camino de los Descubrimientos, Sevilla 41092 (Spain)
[d] D. Rodríguez-Padrón, Dr. R. Luque
Department of Organic Chemistry
IUNAN, UCO
Campus Universitario de Rabanales, Córdoba 14014 (Spain).
E-mail: q62alsor@uco.es
[e] Dr. A. R. González-Elipe
Laboratory of Nanotechnology on Surfaces
Instituto de Ciencia de Materiales de Sevilla (CSIC-USE).
Avda. Américo Vespucio, Sevilla 41092 (Spain)
[f] Dr. R. Luque
Peoples Friendship University of Russia (RUDN University)
6 Miklukho-Maklaya str., Moscow (Russia)

Supporting information for this article is given via a link at the end of the document.

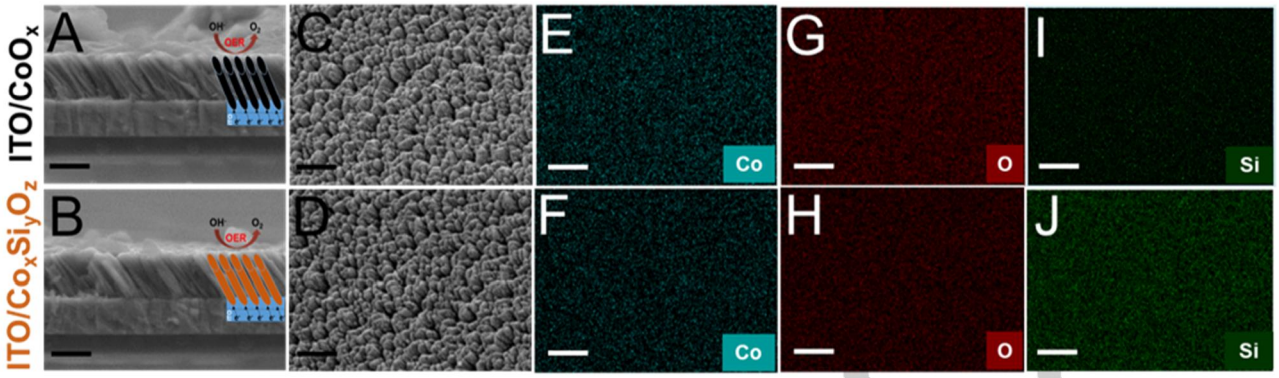

Figure 1. (A, B) Cross-section and (C, D) top-view SEM images of the CoO_x and $Co_xSi_yO_z$ layers (scale bar: 500 nm). Inset on (A, B): Schematic representation of the CoO_x and $Co_xSi_yO_z$ nanowires onto ITO substrate. (E-J) SEM-EDX mapping for Co, O and Si of both layers.

film exhibited a higher silicon content, in comparison with the observed Co content, that confers a greater mechanical stability to the layer. As shown in Figure 1E-J, Co, Si and O are homogeneously distributed on the surface of the samples.

X-ray photoelectron spectroscopy (XPS) analysis was performed to get more insights about the chemical composition of the prepared materials. XPS spectrum of the Co-based sample revealed the presence of carbon, oxygen and cobalt. Carbon band, centered at 284.6 eV (Figure 2A), could be attributed to the presence of graphitic carbon. Figure 2C showed a peak at 780.8 eV, which indicates the formation of cobalt oxide, with the presence of both Co^{2+} and Co^{3+} species. In addition, O 1*s* signal (Figure 2B) could be deconvoluted in two peaks at 529.9 and 531.4 eV, associated with O-metal and O-O bonds, respectively. Particularly, the O-metal band further confirmed the formation of cobalt oxide. On the other hand, XPS measurements of the Co/Si-based material, clearly indicated the presence of Si, related to the Si 2*s* peak at 153.2 eV (Figure 2D). Additionally, carbon band at 284.6 eV, assigned to graphitic carbon, was also visualized, as shown in Figure 2E. The presence of Co $2p_{1/2}$ band at 780.5 eV, suggested the presence of cobalt oxide in the sample, as previously described for the Co-based material (Figure 2G). As the valance state of Co in the electrocatalyst has a great influence on its resulting OER performance (i.e. high Co charge state promotes the OER),[32] the relative mole ratio of Co^{3+}/Co^{2+} of both materials was calculated as 0.7:1 for CoO_x (Figure 2C) and 1.1:1 for $Co_xSi_yO_z$ (Figure 2G). These results indicate that, although the total amount of Cobalt in CoO_x layer is higher than in $Co_xSi_yO_z$, the proportion of Co^{3+} in the latter is higher than in the former case. It suggests that the addition of Si could be profitable to favor the electron transfer and to improve both the activity and chemical stability of the catalyst.[33] Quantification analysis of the atomic composition on the surface of the material revealed an atomic Si/Co ratio of 1.75 (or an atomic Co/Si ratio of 0.57). Moreover, oxygen signal also displayed two contributions at 531.5 and 530.0 eV associated with O-O and O-Co bonds, respectively (Figure 2 F).

X-Ray Diffraction (XRD) analysis was carried out for both samples to infer the effect of the silicon on the crystal structure of the cobalt oxide. The resulting XRD patterns are shown in Figure 3. The main diffraction peaks at 18.99º, 36.84º, 55.64º and 65.22º are assigned to Co_3O_4 for both layers (JCPDS Card no. 09-0418), whilst the other ones are characteristic of the ITO substrate (JCPDS Card no. 89-4597).[34] Interestingly, the addition of silicon to the layer does not modify the crystal character of the Cobalt, which stays as Co_3O_4 in all cases, indicating the absence of

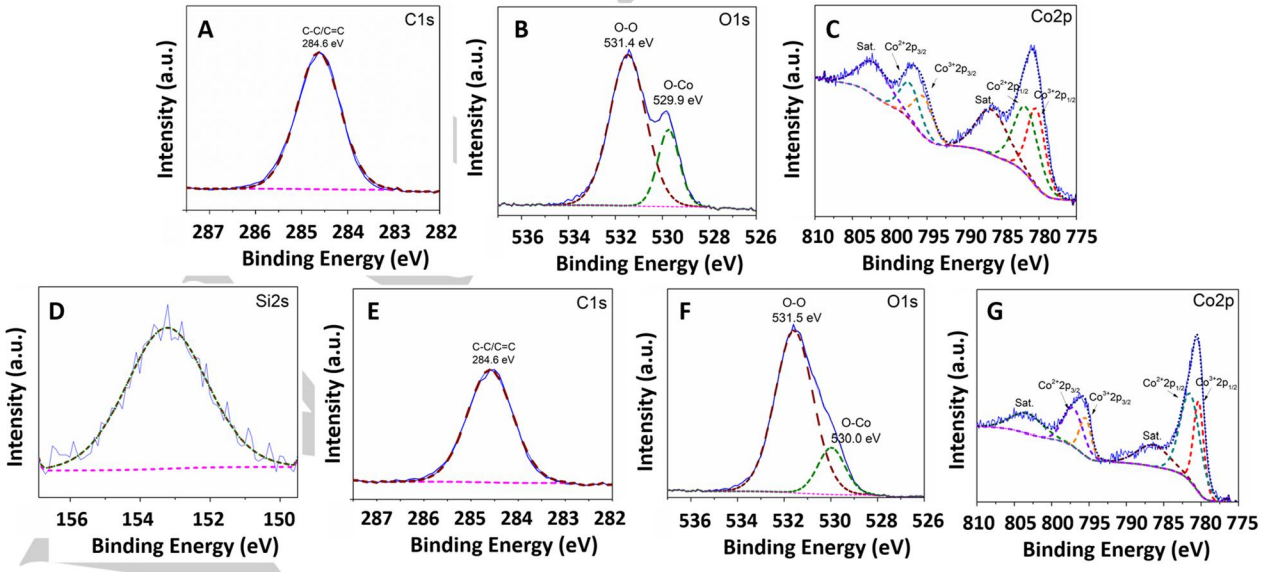

Figure 2. Deconvoluted XPS spectra of CoO_x layer in the (A) C 1*s*, (B) O 1*s* and (C) Co 2*p* XPS regions. Deconvoluted XPS spectra of $Co_xSi_yO_z$ layer in the (D) Si 2*s*, (E) C 1*s*, (F) O 1*s* and (G) Co 2*p* XPS regions.

charge redistribution in the doping structure. It is worth noting that heteroatom doping is a promising method to modify the properties of host materials for energy related applications.[35] In this case, the functionality of Si-dopant heteroatom is mainly used to improve the mechanical and chemical stability of the resultant doped structure.

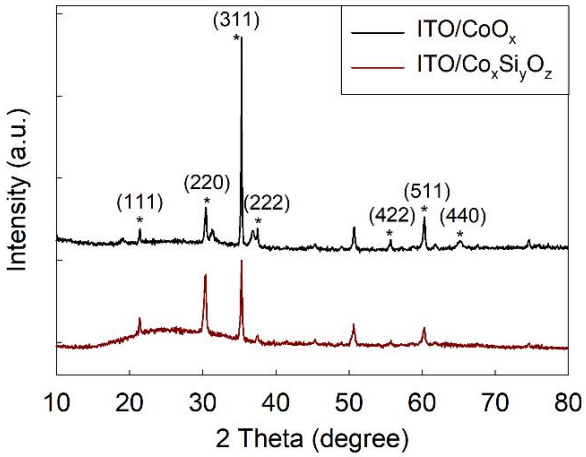

Figure 3. XRD patterns of the ITO/CoOx and ITO/CoxSiyOz layers.

The electrochemical properties of the porous CoO_x and $Co_xSi_yO_z$ nanowires as OER electrocatalysts were assessed. Figure 4A shows the linear sweep voltammetric (LSV) curves, without IR correction, obtained on bare-ITO, ITO/CoO_x and ITO/$Co_xSi_yO_z$ electrodes measured in O_2-saturated 0.5 M KOH aqueous electrolyte, and at 80 ºC. As shown, the bare ITO electrode exhibits negligible anodic current density in the study potential range (vs. RHE). Whilst ITO/CoO_x and ITO/$Co_xSi_yO_z$ electrodes show a significative electrocatalytic response for OER. Table 1 summarizes the resulting onset potential (E_{onset}), overpotential at 10 mA·cm^{-2} (η) and Tafel slope values for both deposition layers, which were obtained from Figure 4A and 4B, respectively. Although the Tafel slopes of both electrodes were almost identical,

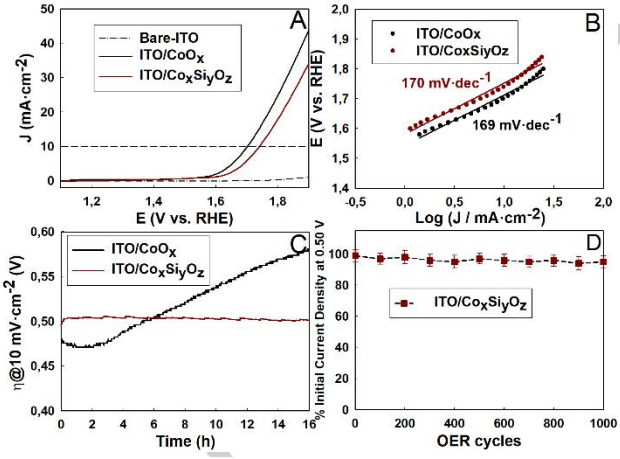

Figure 4. (A) LSV curves of Bare-ITO and ITO modified both with CoO_x and $Co_xSi_yO_z$ layers in O_2-saturated 0.5 M KOH at 80 ºC; (B) Tafel polarization curves obtained from (A). OER durability tests: (C) Chronopotentiometric measurement of both porous layers at 10 mA·cm^{-2} for 16 h.; (D) Monitoring percentage of initial current density after 1000 chronoamperometric cycles at a constant overpotential of 0.50 V with the ITO/$Co_xSi_yO_z$ electrode.

which means non significative differences in their electrocalytic activity, ITO/CoO_x presents better E_{onset} and η values than ITO/$Co_xSi_yO_z$. The latter difference can be attributed to the higher amount of Cobalt on the former electrode. On the other hand, the OER electrochemical performance parameters of ITO/CoO_x and ITO/$Co_xSi_yO_z$ electrodes were even better than the recently reported for hierarchical cobalt oxide-functionalized silicon carbide nanowire electrode, e.g., a Tafel slope of 320 mV·dec^{-1}.[36] Long-term stability analysis was performed by chronopotentiometry at a current density of 10 mA·cm^{-2} for 16 h. Surprisingly, as it can be observed in Figure 4C, only the overpotential of the ITO/$Co_xSi_yO_z$ electrode remained almost constant for 16 h., whilst the overpotential of the ITO/CoO_x electrode increased over time. This fact was mainly due to the progressive loss of the CoO_x material on the ITO surface (see Figure S1), demonstrating that the presence of silicon on the mixed oxide network is beneficial for the stability of the film, simultaneously maintaining the good electrocatalytic properties. To further investigate the durability of the ITO/$Co_xSi_yO_z$ electrode, a deterioration experiment was performed by applying 1000 OER cycles. Figure 4D shows that the percentage of the initial current density was maintained almost constant after 1000 cycles, demonstrating the excellent long-term stability of the $Co_xSi_yO_z$ layer. And according the figure of merit for OER electrocatalysts in the review article reported by Tahir et al.,[1] ITO/$Co_xSi_yO_z$ is considered as a good OER catalyst in comparison with the literature. Furthermore, the integrity of the $Co_xSi_yO_z$ film after long testing in KOH is demonstrated by comparing the difraction patterns of this layer before and the test (Figure S2).

Table 1. OER electrocatalytic parameters obtained from Figure 4.

Electrode	E_{onset} (V)	η (mV) at 10 mA·cm^{-2}	Tafel slope (mV-dec^{-1})
ITO/CoO_x	1.57	470	169
ITO/$Co_xSi_yO_z$	1.59	500	170

In summary, we have demonstrated that ITO/$Co_xSi_yO_z$ electrode fabricated by a chemical vapor deposition modality (MS-GLAD) provides similar OER electrocatalytic performance that its counterpart made in the absence of silicon (i.e. ITO/CoO_x one), despite of the different Cobalt content, which was around 2-fold lower in the former layer. In addition, the obtained results confirmed that the inclusion of Si in the $Co_xSi_yO_z$ layer slightly modifies the electronic structure of the cobalt oxide by increasing the valance state of its Co atoms,[37] which not only provides a positive effect on its catalytic activity but also greatly enhances the long-term stability for OER of the doped structures.[33] This work pays the way to study other possible configurations by MS-GLAD configuration, such as higher ratios both of Co/Si and

Co^{3+}/Co^{2+}, layer thickness, deposition substrate, that could significatively enhance the OER electrocatalytic performance of these thin film based-materials.

Experimental Section

Instrumentation.

SEM and EDX images were acquired in the JEOL-SEM JSM-7800 LV scanning microscope. XPS experiments were accomplished in an ultrahigh vacuum multipurpose surface analysis instrument SpecsTM. The samples were evacuated overnight under vacuum (10^{-6} Torr) and subsequently, measurements were performed at room temperature using a conventional X-ray source with a Phoibos 150-MCD energy detector. XPS spectra were analysed employing the XPS CASA software. XRD experiments were performing using a Bruker D8 ADVANCE diffractometer operating at 40 kV and 40 mA, using Cu Kα radiation (1.5406 A).

Thin Films preparation

All films were deposited using the same experimental conditions. The magnetron operated with a power of 100 W and a pulsed voltage of 250-400 V at a frequency of 80 kHz. The base pressure of the system was $3.0 \cdot 10^{-9}$ bar. The pressure during deposition was fixed at $5.0 \cdot 10^{-6}$ bar. The distance and the films growth angle between ITO substrate and target were 5 cm and 80º, respectively. The porous $Co_xSi_yO_z$ and CoO_x layers were deposited using a 50 mm diameter Co/Si (75/25 wt%) and Co targets, respectively. In all cases, depositions were carried out using a ϕ_{O2}/ϕ_{Ar} = 0.1. The deposition time was adjusted to obtain the same thickness on both films.

Acknowledgements

Support from the Ministry of Economy and Competitiveness (MINECO) of Spain is acknowledged through the MANA project CTQ2017-83961-R. J.J.G.-C. acknowledges the MINECO for a “Ramon y Cajal” contract (#RyC-2014-14956). M.C. and F.J.G.-G. thank the “Plan Propio de Investigación” from the Universidad de Córdoba (UCO) and the “Programa Operativo de fondos FEDER Andalucía” for its financial support through both postdoctoral contracts (Modality 5.2.A). The publication has been prepared with support from RUDN University Program 5-100. R. Luque gratefully acknowledges MINECO for funding project CTQ2016-78289-P, co-financed with FEDER funds. A.R. Puente-Santiago gratefully acknowledge MINECO for their research contracts associated to the aforementioned project, and to the Research Program of the UCO for its financial support through a postdoctoral contract (Modality 5.1). Francisco García-Alfonso, Rocío Vargas-Díaz and Vicente Montes-Jiménez are acknowledged for their assistance with the SEM analysis.

Conflict of Interest

The authors declare no conflict of interest.

Keywords: $Co_xSi_yO_z$ • Cobalt oxide • Electrocatalysis • Oxygen evolution reaction • Water splitting

[1] M. Tahir, L. Pan, F. Idrees, X. Zhang, L. Wang, J.-J. Zou, Z. L. Wang, *Nano Energy* **2017**, *37*, 136–157.
[2] N.-T. Suen, S.-F. Hung, Q. Quan, N. Zhang, Y.-J. Xu, H. M. Chen, *Chem. Soc. Rev.* **2017**, *46*, 337–365.
[3] H. Zhong, C. Campos-Roldán, Y. Zhao, S. Zhang, Y. Feng, N. Alonso-Vante, *Catalysts* **2018**, *8*, 559.
[4] H. Wang, Y. Liang, Y. Li, H. Dai, *Angew. Chemie Int. Ed.* **2011**, *50*, 10969–10972.
[5] S. Dou, L. Tao, J. Huo, S. Wang, L. Dai, *Energy Environ. Sci.* **2016**, *9*, 1320–1326.
[6] H. Zhang, T. Wang, A. Sumboja, W. Zang, J. Xie, D. Gao, S. J. Pennycook, Z. Liu, C. Guan, J. Wang, *Adv. Funct. Mater.* **2018**, *28*, 1804846.
[7] T. Maiyalagan, K. A. Jarvis, S. Therese, P. J. Ferreira, A. Manthiram, *Nat. Commun.* **2014**, *5*, 3949.
[8] H. Jin, J. Wang, D. Su, Z. Wei, Z. Pang, Y. Wang, *J. Am. Chem. Soc.* **2015**, *137*, 2688–2694.
[9] W. Xu, F. Lyu, Y. Bai, A. Gao, J. Feng, Z. Cai, Y. Yin, *Nano Energy* **2018**, *43*, 110–116.
[10] T. Y. Ma, S. Dai, M. Jaroniec, S. Z. Qiao, *J. Am. Chem. Soc.* **2014**, *136*, 13925–13931.
[11] Y.-Z. Chen, C. Wang, Z.-Y. Wu, Y. Xiong, Q. Xu, S.-H. Yu, H.-L. Jiang, *Adv. Mater.* **2015**, *27*, 5010–5016.
[12] Q. Shi, S. Fu, C. Zhu, J. Song, D. Du, Y. Lin, *Mater. Horizons* **2019**, *6*, 684–702.
[13] G. Fan, F. Li, D. G. Evans, X. Duan, *Chem. Soc. Rev.* **2014**, *43*, 7040–7066.
[14] S. Zhang, Y. Zhang, W. Jiang, X. Liu, S. Xu, R. Huo, F. Zhang, J.-S. Hu, *Carbon N. Y.* **2016**, *107*, 162–170.
[15] X. Xu, Z. Zhong, X. Yan, L. Kang, J. Yao, *J. Mater. Chem. A* **2018**, *6*, 5999–6006.
[16] Z.-S. Wu, W. Ren, L. Wen, L. Gao, J. Zhao, Z. Chen, G. Zhou, F. Li, H.-M. Cheng, *ACS Nano* **2010**, *4*, 3187–3194.
[17] Y. Liang, Y. Li, H. Wang, J. Zhou, J. Wang, T. Regier, H. Dai, *Nat. Mater.* **2011**, *10*, 780–786.
[18] M. Li, C. Bao, Y. Liu, J. Meng, X. Liu, Y. Cai, D. Wuu, Y. Zong, T.-P. Loh, Z. Wang, *RSC Adv.* **2019**, *9*, 16534–16540.
[19] T. Zhang, C. He, F. Sun, Y. Ding, M. Wang, L. Peng, J. Wang, Y. Lin, *Sci. Rep.* **2017**, *7*, 43638.
[20] H. Li, X. Li, H. Lei, G. Zhou, W. Zhang, R. Cao, *ChemSusChem* **2019**, *12*, 801–806.
[21] T. Ouyang, Y.-Q. Ye, C.-Y. Wu, K. Xiao, Z.-Q. Liu, *Angew. Chemie Int. Ed.* **2019**, *58*, 4923–4928.
[22] L. Wu, Q. Li, C. H. Wu, H. Zhu, A. Mendoza-Garcia, B. Shen, J. Guo, S. Sun, *J. Am. Chem. Soc.* **2015**, *137*, 7071–7074.
[23] D. T. Gillaspie, R. C. Tenent, A. C. Dillon, *J. Mater. Chem.* **2010**, *20*, 9585.
[24] E. Amasawa, N. Sasagawa, M. Kimura, M. Taya, *Adv. Energy Mater.* **2014**, *4*, 1400379.
[25] F. Grote, Z.-Y. Yu, J.-L. Wang, S.-H. Yu, Y. Lei, *Small* **2015**, *11*, 4666–4672.
[26] P. Yang, P. Sun, W. Mai, *Mater. Today* **2016**, *19*, 394–402.
[27] J. Gil-Rostra, F. García-García, F. Yubero, A. R. González-Elipe, *Sol. Energy Mater. Sol. Cells* **2014**, *123*, 130–138.
[28] F. J. Garcia-Garcia, J. Gil-Rostra, F. Yubero, A. R. González-Elipe, *Nanosci. Nanotechnol. Lett.* **2013**, *5*, 89–93.
[29] J. Gil-Rostra, M. Cano, J. M. Pedrosa, F. J. Ferrer, F. García-García, F. Yubero, A. R. González-Elipe, *ACS Appl. Mater. Interfaces* **2012**, *4*, 628–638.
[30] F. J. Garcia-Garcia, J. Gil-Rostra, F. Yubero, J. P. Espinós, A. R. Gonzalez-Elipe, J. Chaboy, *J. Phys. Chem. C* **2015**, *119*, 644–652.
[31] F. J. Garcia-Garcia, F. Yubero, J. P. Espinós, A. R. González-Elipe, R. M. Lambert, *J. Power Sources* **2016**, *324*, 679–686.
[32] Y. Zhao, B. Jin, Y. Zheng, H. Jin, Y. Jiao, S.-Z. Qiao, *Adv. Energy Mater.* **2018**, *8*, 1801926.
[33] H. Jin, X. Liu, Y. Jiao, A. Vasileff, Y. Zheng, S.-Z. Qiao, *Nano Energy* **2018**, *53*, 690–697.
[34] D. Alba-Molina, A. R. Puente Santiago, J. J. Giner-Casares, M. T. Martín-Romero, L. Camacho, R. Luque, M. Cano, *J. Phys. Chem. C* **2019**, *123*, 9807–9812.
[35] H. Jin, X. Liu, S. Chen, A. Vasileff, L. Li, Y. Jiao, L. Song, Y. Zheng, S.-Z. Qiao, *ACS Energy Lett.* **2019**, *4*, 805–810.
[36] C.-P. Lee, L. E. Luna, S. DelaCruz, S. Ortaboy, F. Rossi, G. Salviati, C. Carraro, R. Maboudian, *Mater. Today Energy* **2018**, *7*, 37–43.
[37] H. Jin, X. Liu, A. Vasileff, Y. Jiao, Y. Zhao, Y. Zheng, S.-Z. Qiao, *ACS Nano* **2018**, *12*, 12761–12769.

Entry for the Table of Contents (Please choose one layout)

Layout 1:

COMMUNICATION

Highly stable silicon-cobalt mixed oxide thin film with a porous columnar nanostructure structure displays excellent long-term stability as electrocatalyst for OER, maintaining a suitable electrocatalytic response.

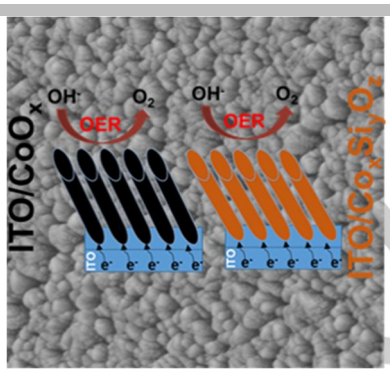

Manuel Cano, Francisco J. Garcia-Garcia, Daily Rodríguez-Padrón, Agustín R. González-Elipe, Juan J. Giner-Casares and Rafael Luque**

Page No. – Page No.

Ultrastable CoxSiyOz Nanowires by Glancing Angle Deposition with Magnetron Sputtering as Novel Electrocatalyst for Water Oxidation

Layout 2:

COMMUNICATION

((Insert TOC Graphic here))

*Author(s), Corresponding Author(s)**

Page No. – Page No.

Title

Text for Table of Contents